JACS
JOURNAL OF THE AMERICAN CHEMICAL SOCIETY
Article
pubs.acs.org/JACS

Detection of the Short-Lived Cation Radical Intermediate in the Electrochemical Oxidation of *N,N*-Dimethylaniline by Scanning Electrochemical Microscopy

Fahe Cao, Jiyeon Kim, and Allen J. Bard*

Center for Electrochemistry, Department of Chemistry and Biochemistry, University of Texas at Austin, Austin, Texas 78712, United States

Supporting Information

ABSTRACT: The short-lived intermediate *N,N*-dimethylaniline (DMA) cation radical, $DMA^{\bullet+}$, was detected during the oxidation of DMA in MeCN with 0.1 M tetra-*n*-butylammonium hexafluorophosphate. The detection was accomplished at steady state by scanning electrochemical microscopy (SECM) with ultramicroelectrodes using the tip generation/substrate collection mode. Cyclic voltammetry (CV) with a 2 mm Pt electrode indicates that DMA oxidation in acetonitrile is followed by a dimerization and two electrochemical reactions, which is consistent with previous results. The $DMA^{\bullet+}$ intermediate is detected by SECM, where the $DMA^{\bullet+}$ generated at the ca. 500 nm radius Pt tip is collected on a 5 μm radius Pt substrate when the gap between the tip and the substrate is a few hundred nanometers. Almost all of the $DMA^{\bullet+}$ is reduced at the substrate when the gap is 200 nm or less, yielding a dimerization rate constant of 2.5×10^8 $M^{-1}\cdot s^{-1}$ based on a simulation. This is roughly 3 orders of magnitude larger than the value estimated by fast-scan CV. We attribute this discrepancy to the effects of double-layer capacitance charging and adsorbed species in the high scan rate CV.

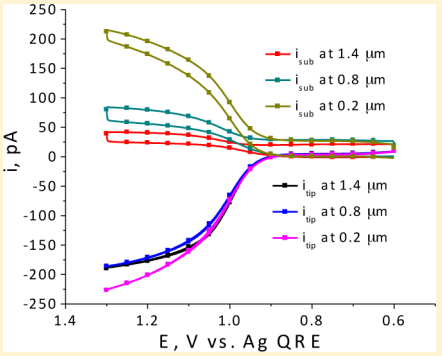

INTRODUCTION

In determining the mechanism of electrode reactions, it is often helpful to detect and characterize the product of the initial electron-transfer reaction. In many cases, the product of a one-electron transfer reacts rapidly, for example by a proton transfer or dimerization reaction. An ongoing challenge has been increasing the speed of the electrochemical measurement so that very unstable intermediates, e.g., those with lifetimes of less than a microsecond, can be detected. One technique that has been developed is fast-scan cyclic voltammetry (FSCV), where an ultramicroelectrode (UME) is used to decrease contributions from capacitance. However, FSCV suffers from limitations at a high scan rate because contributions from adsorbed species and electrode surface processes interfere. Moreover, using a single electrode for generating the species and detecting it requires switching delays and complicates the measurement. We contend that a measurement made at steady state and with two electrodes—one that generates the intermediate of interest and one that collects (or detects) it as it traverses a small gap—as in scanning electrochemical microscopy (SECM), is a simpler measurement that can be simulated with high accuracy.

We report here a study of a classic reaction, the oxidation of *N,N*-dimethylaniline (DMA) to *N,N,N,N*-tetramethylbenzidene (TMB), by the detection of the cation radical in MeCN and the determination of its dimerization rate by SECM. The oxidation of anilines in aqueous and nonaqueous solutions often leads to the formation of a conducting film, and the anodic behavior of anilines and the electrochemical, electrical, and physicochemical properties of polyaniline films have been presented in previous studies.[1−14] Early studies by Adams and co-workers[13,15−17] indicated that the anodic oxidation of aniline and its derivatives in aqueous and nonaqueous solutions usually occurred via a series of reactions and resulted in a large number of products, depending on the reaction conditions. Parker studied the oxidation of DMA with different para-substituents by CV and proposed that there was no reversible potential of DMA oxidation because of the rapid consumption of the $DMA^{\bullet+}$ by following chemical reactions. Based on linear sweep voltammetry, the second-order rate constants for the $DMA^{\bullet+}$ cation radical reacting with acetate ion ranged from 3.2×10^6 $M^{-1}\cdot s^{-1}$ for the *p*-methoxy-substituted cation radical to 3×10^9 $M^{-1}\cdot s^{-1}$ for the corresponding *p*-nitro derivative.[5] In our previous work, FSCV was used to investigate the mechanism of the anodic oxidation of DMA in acetonitrile solution.[14] Based on FSCVs and digital simulation, a rate constant of 6.3×10^5 $M^{-1}\cdot s^{-1}$ was found for the second-order cation radical coupling with a following deprotonation reaction:

$$DMA - e^- \rightleftharpoons DMA^{\bullet+} \quad (1)$$

$$2DMA^{\bullet+} \rightarrow TMB + 2H^+ \quad (2)$$

$$TMB - e^- \rightleftharpoons TMB^{\bullet+} \quad (3)$$

Received: November 11, 2014
Published: December 5, 2014

$$TMB^{\bullet+} - e^- \rightleftharpoons TMB^{2+} \quad (4)$$

FSCV has been used previously with other systems to resolve single-electron-transfer steps in two-electron- and multi-electron-transfer reactions and to detect unstable intermediates in electrochemical reactions.[18] As mentioned, a difficulty of FSCV is the complexity of dealing with capacitance due to double-layer charging and faradaic current due to adsorbed species at high scan rates (v). Since the current caused by these surface processes increases linearly with v, while that of diffusion-controlled electrochemical reactions increases in proportion to $v^{1/2}$, the former dominates at larger v.[18,19] A rotating ring-disk electrode (RRDE) was also applied to study the electro-oxidation of DMA in strong acidic aqueous solution.[17,20] Since construction of an RRDE is difficult, a high rotation rate is required to effect interelectrode transport, which is not required for SECM. The principles of SECM, i.e., generation at one electrode and collection at another, are analogous to those employed in the RRDE study. However, the approach curves or CVs at different fixed distances have the advantage of larger collection efficiencies, larger fluxes between electrodes, and the ability to vary continuously the interelectrode spacing.

SECM has been used as a powerful tool to detect intermediates for over 20 years.[18,21−23] Tip generation/substrate collection (TG/SC) voltammograms for the reduction of acrylonitrile showed the electrogeneration of the anion radical with a 5 μm diameter Au tip and a 60 μm diameter Au substrate.[21] Chang applied FSCV and SECM to investigate the reduction of Sn(IV) bromide and detected the Sn(III) intermediate with a 10 μm diameter Au tip and a 50 μm diameter Au substrate.[18] SECM with nanometer gaps was also applied to study guanosine in dimethylformamide, and it was possible to detect its cation radical with a 10 μm diameter carbon tip and substrate in aqueous solution.[23]

In the current study, SECM was applied to study the electro-oxidation of DMA in MeCN in conjunction with normal CV. TG/SC mode with Pt UMEs of ca. 0.5 μm radius (a) for the tip and a = 5 μm for the substrate was applied to detect the short-lived cation radical formed in DMA electro-oxidation, and the kinetic parameters were determined by fitting the collection efficiency at different interelectrode distances to a simulation. The operating principle of the TG/SC mode in SECM for the DMA electrochemical oxidation study is illustrated in Figure 1. Route 1 is the dimerization of $DMA^{\bullet+}$ radicals to form TMB, and then TMB can be further oxidized at the tip at a larger d. As d decreases, more and more radicals are captured, as shown in route 2. To the authors' knowledge, no nanogap SECM experiments with tip and substrate electrodes this small (a = 0.5 μm tip and a = 5 μm substrate) have been conducted for the detection of a cation radical in nonaqueous solution.

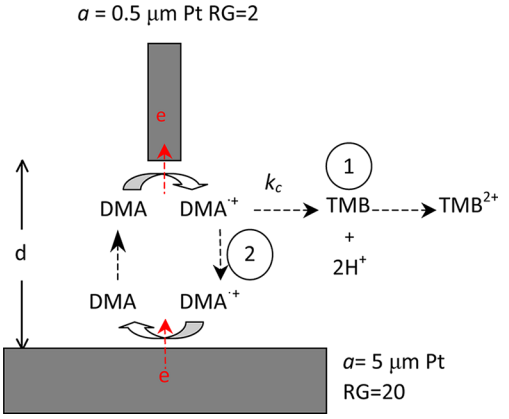

Figure 1. Schematic depiction of the collection of the unstable $DMA^{\bullet+}$ radical cation in TG/SC mode of SECM. When the tip is far from the substrate, route 1, the dimerizationof $DMA^{\bullet+}$ to TMB leads to electron-transfer reactions on the tip and substrate. For a smaller gap between tip and substrate, route 2, more and more $DMA^{\bullet+}$ can be captured by reduction at the substrate electrode.

EXPERIMENTAL SECTION

Chemicals and Materials. *N,N*-Dimethylaniline (DMA, 99%, Acros Organics, New Jersey), ethyl viologen perchlorate (EVD, Sigma-Aldrich, St. Louis, MO), and ferrocenemethanol (FcMeOH, 97%, Acros Organics, NJ) were used as received. Tetra-*n*-butylammonium hexafluorophosphate ($TBAPF_6$, Sigma-Aldrich, St. Louis, MO) was chosen as supporting electrolyte. Acetonitrile (MeCN, Acros Organics, NJ) was used as received, but about 0.5 g of ICN Alumina N-Super 1 (ICN Biomedicals, Costa Mesa, CA) was added to the solution of MeCN for further drying. Other chemicals were reagent grade and were used as received. All aqueous solutions were prepared with deionized Milli-Q water.

Before the addition of DMA and EVD to the MeCN with $TBAPF_6$ supporting electrolyte, the solution was purged with argon for about 10 min until the background CV (checked by potential sweeps between 2.0 and −2.0 V) was flat. The solution was purged by argon during the CV experiment. For the SECM experiments, a glovebag was used to keep the system free of oxygen.[24] When the collection efficiency and approach curves were measured using SECM, no argon was pumped into the glovebag. Otherwise, the glovebag was continuously purged with argon.

Instrumentation and Measurement. CV and SECM experiments were performed with a CHI920 SECM bipotentiostat (CH Instruments, Austin, TX). Three electrodes were used for normal CV: a Pt electrode (2 mm diameter) as a working electrode, a Pt wire as a counter electrode, and a silver wire as quasi-reference electrode (QRE). Four electrodes were used in SECM experiments: ca. a = 0.5 μm Pt UME with RG = 2 as a tip, a = 5 μm Pt UME with RG = 20 as a substrate electrode, and the same counter and reference electrodes as the CV experiments.

Pt UME Fabrication. The 10 μm diameter platinum wire from Alfa Aesar (Mard Hill, MA) and a borosilicate capillary with 1.5 mm outer diameter and 0.75 mm inner diameter from FHC (Bowdoin, ME) were used to fabricate the 10 μm diameter UME. All were prepared by procedures described elsewhere.[25] Approximately a = 0.5 μm Pt tips with small RG (ratio of the radius of the tip that includes the glass sheet to that of the Pt wire) of 2 were fabricated as reported elsewhere, especially by the Amemiya group.[26−29] A laser puller (P-2000, Sutter Instruments Co., Novato, CA) with three different programs was used to fabricate smaller Pt wires sealed in glass. The glass layer surrounding the tip fabricated by laser puller was heated over the Pt coil heater of a Micro Forge (MF-900, Narishige, Tokyo, Japan) to melt it and retract it from the tip. A sharp tip with desirable inner and outer radii was obtained by focused ion beam (FIB) milling (scanning electron microscopy (SEM)/FIB FEI Strata DB235 SEM/FIB with Zyvex S100) of the heat-annealed tip across the meniscus region of the glass layer.[30] The final result was a disk shaped a = 0.5 μm Pt tip with RG = 2 as shown Supporting Information, Figure S1a, which is an electron beam image of the tip at 52° tilt.

Electrochemical characterization of the obtained sub-micrometer electrode was performed by means of CV using a three-electrode configuration. Assuming a non-recessed, disk-shaped sub-micrometer electrode, estimation of the electrode radius can be done based on the steady-state current from CV at a scan rate of 50 $mV{\cdot}s^{-1}$ in 1 mM FcMeOH aqueous solution containing 0.1 M KNO_3 as supporting electrolyte, as shown in Supporting Information, Figure S1b. The steady-state current of FcMeOH oxidation at 0.45 V vs Ag/AgCl was

149 pA, and the radius for the tip was calculated to be 0.49 μm based on the following formula,[31]

$$i_{ss} = 4nFDca$$

where i_{ss} is the steady-state current, n is the number of electrons (n = 1 for FcMeOH oxidation), F is the Faraday constant (96 500 C·mol^{-1}), D is the diffusion coefficient (7.8 × 10^{-6} cm^2·s^{-1} for FcMeOH in 0.1 M KNO_3 aqueous solution[32,33]), c is the concentration of FcMeOH, and a is the radius of the UME. This result is consistent with an SEM image of the tip.

The average values are consistent with values determined from approach curves to a conductive substrate,[34] which agree very well with the corresponding theoretical curve obtained from the COMSOL fitting, as shown in Supporting Information, Figure S1c. Note that no contact between the tip and smooth glassy carbon substrate occurs at a very short distance d of L < 0.2 (d/a, L = 0.2 and d = 100 nm for a = 500 nm with RG = 2.1 in Figure S1c). The result confirms that the FIB-milled tip is smooth and perpendicularly aligned with respect to the tip length.

RESULTS AND DISCUSSION

CV of DMA in MeCN. Figure 2 shows the typical CVs of DMA obtained at a 2 mm platinum disk electrode in MeCN

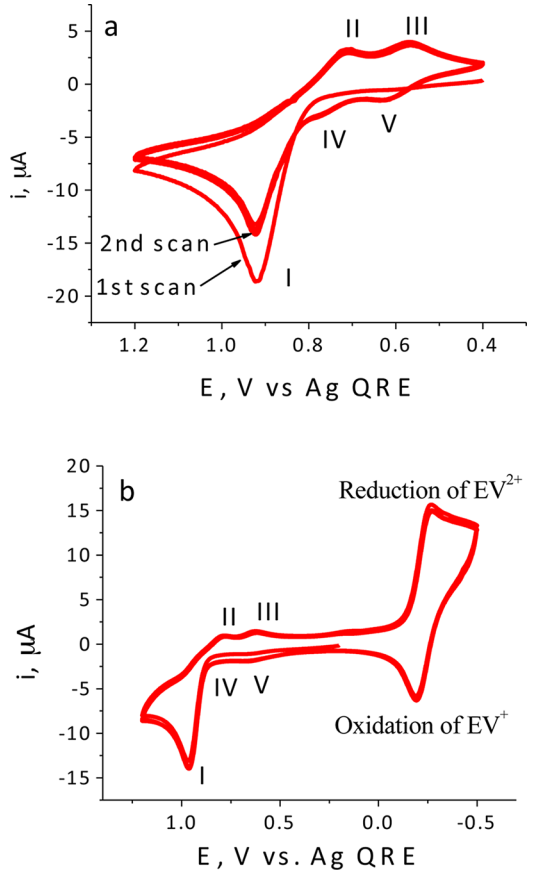

Figure 2. CVs of 0.5 mM DMA in acetonitrile (a) with 0.1 M tetra-*n*-butylammonium hexafluorophosphate as supporting electrolyte and (b) with 1.2 mM ethyl viologen perchlorate at a 2 mm diameter Pt electrode at a scan rate of 50 mV·s^{-1}.

containing 0.1 M $TBAPF_6$ supporting electrolyte at low scan rate (v = 50 mV·s^{-1}) with and without 1.2 mM EVD, which serves as a potential reference and redox mediator for further approach experiments. The CVs show only one peak on the first positive scan at a potential of ca. 0.92 V (vs Ag QRE)

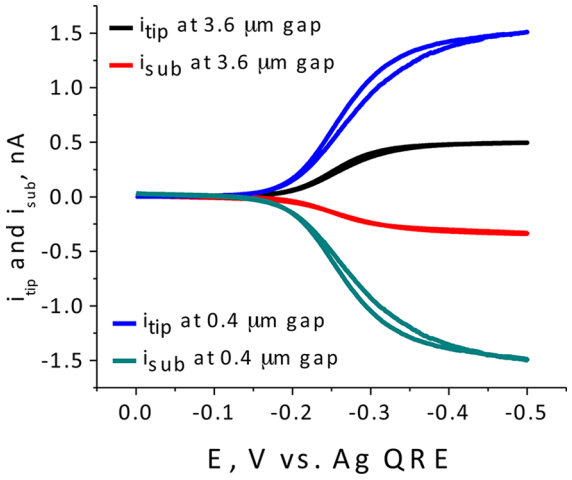

Figure 3. Collection of 1 mM EVD at different tip to substrate distances. The tip potential is scanned from 0 to −0.5 V at a scan rate of 20 mV·s^{-1}, while the substrate potential is fixed at 0 V. The result indicates low collection efficiency (66%) with the bigger gap (3.6 μm), while it is 100% with the smaller gap (0.4 μm).

without a reversal peak in the negative scan, while several new peaks are observed in the negative scan and the second positive scan (Figure 2). In further scans, those peaks labeled I, II, III, IV, and V are stable, indicating no polymer film formed on the Pt electrodes. As shown in previous studies from Adams[13,16,17] and our group,[14] peaks II, IV and III, V represent two new redox couples, namely TMB oxidation to form a stable dication as shown in eqs 1−4 and route 1 in Figure 1. With additional EVD, the curves between 0.4 and 1.2 V are almost the same as shown in Figure 2a, while there is a well-defined redox reaction of EVD in the potential range of 0 to −0.5 V vs Ag QRE that does not interfere with DMA oxidation. Therefore, EVD can be used as redox mediator for determining the distance between the tip and substrate in nonaqueous solution. Previous research has shown no direct evidence of the $DMA^{\bullet+}$ radical cation due to the high rate constant of the dimerization reaction in eq 2 and the high charging current of FSCV. In the current study, we applied the TG/SC mode of SECM with nanometer gap and sub-micrometer Pt UME to (1) examine the mechanism of DMA oxidation in detail and prove the existence of the $DMA^{\bullet+}$ cation radical at steady state and (2) estimate the lifetime of the radical and the kinetic parameters of the homogeneous radical ion coupling reaction.

Alignment of a = 0.5 μm Tip to a = 5 μm Substrate Using EVD in Nonaqueous Solution. Typical CVs of 1 mM EVD in MeCN with 0.1 M $TBAPF_6$ as supporting electrolyte for 0.5 and 5 μm radius Pt UMEs are shown in Supporting Information, Figure S2. Well-defined diffusion-limited currents of 322 pA and 3.4 nA for a = 0.5 and 5 μm Pt UMEs, respectively, indicate that those two electrodes are well-constructed, with no recess of the Pt and no gap between the Pt and the glass. This conclusion is also confirmed by the UME image and the approach curve shown in Supporting Information, Figure S1. Due to the large background current of a large substrate electrode in TG/SC experiments, a = 5 μm Pt UME was chosen as a substrate to decrease the background current relative to the very small a = 0.5 μm UME tip. Combined with CCD camera microscopy (Infinity2-1, Caltex lens VZ-400, Ontario, Canada), a typical x and y axis scanning curve is shown in the Supporting Information, Figure S3, where

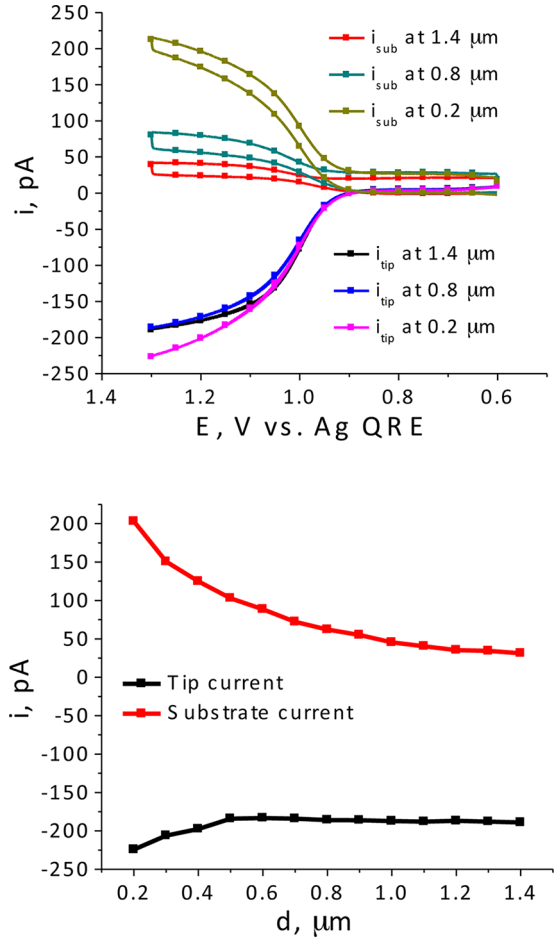

Figure 4. (a, top) Typical collection curves of 0.4 mM DMA oxidation in acetonitrile solution at different gap distances (1.4, 0.8, and 0.2 μm). (b, bottom) Tip and corresponding substrate collection currents of all collection experiment when the tip potential is 1.3 V vs Ag QRE. The tip potential was swept from 0.6 to 1.3 V vs Ag QRE at a scan rate of 50 mV·s^{-1} to electro-oxidize DMA, while the substrate potential was held at 0.76 V vs Ag QRE to collect the DMA$^{\bullet+}$. The original collection curves are shown in Supporting Information, Figure S5. Baseline subtractions of substrate currents shown in Figure S5 were chosen to obtain those curves and substrate collection currents.

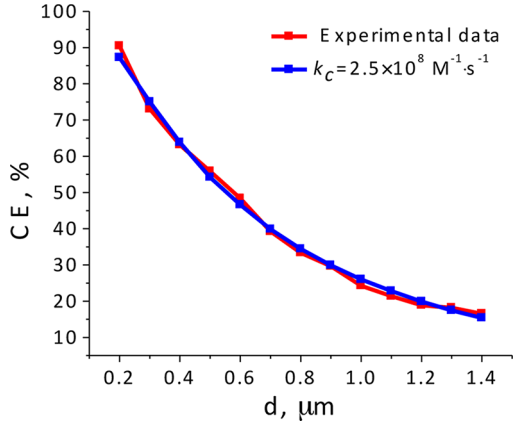

Figure 5. Experimental collection efficiency and the best fit of the results with EC_2EE model simulation. The second-order rate constant (k_c) of the irreversible dimerization reaction is 2.5 × 10^8 M^{-1}·s^{-1}.

E_{tip} and E_{sub} are held at −0.45 and 0 V, respectively. When the tip scans over the substrate, a significant positive feedback peak for the tip can be observed, and a peak collection current on the substrate is also observed both in x- and y-axis scans.[23] The substrate current is much smaller than the tip current due to the large d between the tip and the substrate.

For the SECM approach experiment, EV^{2+} was electro-reduced on the tip and regenerated at the substrate at fixed tip and substrate potentials. A typical approach curve using EVD as a redox mediator in MeCN solution without oxygen is shown in Supporting Information, Figure S4. The E_{tip} was held at −0.45 V to reduce the EV^{2+}, while the E_{sub} was held at 0 V vs Ag QRE, since the reduction of EV^{2+} at −0.45 V is diffusion limited as shown in Supporting Information, Figure S2. The red line represents a theoretical approach curve for a diffusion-limited reaction, derived from a COMSOL simulation. As shown in Figure S4, the experimental approach curve is well in line with the theoretical curve, indicating EVD is a qualified redox mediator for determining the tip to substrate distance and aligning the tip to the substrate. Although there are some slight fluctuations in the curve due to vibrations in the SECM system, the fluctuations are not large enough to prevent good alignment of both the tip and substrate. After aligning the tip and substrate, the collection efficiency (CE) of EVD using the TG/SC mode at different distances was measured. As shown in Figure 3, in the case of a 3.6 μm gap, the CE is around 66%, while the CE is 100% at a smaller gap of 400 nm, which is in line with the simulation results. Due to the large size of the substrate with respect to the small tip electrode and the low scan rate of 20 mV·s^{-1}, a relatively high CE can be found at a large distance (3.6 μm). Significant positive feedback is seen in the tip current, indicating the EVD is a well-defined redox mediator for SECM in nonaqueous solution. Otherwise, the configuration of the 0.5 μm tip and the 5 μm substrate meets the requirements for nanogap tip to substrate separation, and the substrate background current is small enough to observe short-lived radicals using the TG/SC mode of SECM.

Short-Lived Ion Radical Detection by TG/SC Mode of SECM with Nanogap Setup. Even though FSCV was used in our previous work, the short-lived ion radical DMA$^{\bullet+}$ could not be detected very well because of the fast second-order irreversible chemical reaction and a large non-faradic current at very high scan rates (10 000 V·s^{-1}).[14] With TG/SC, a current is measured under a steady-state condition so that clear evidence of DMA$^{\bullet+}$ reduction can be obtained with a reasonably small gap between the tip and the substrate electrodes, d. Figure 4a shows typical curves of the collection of DMA$^{\bullet+}$ in SECM at different d with substrate current baseline subtraction. The original collection curves are shown in Supporting Information, Figure S5, which indicates that even at 10 μm distance, the baseline of substrate current is not horizontal. Baseline subtraction as shown in Figure S5 (green line) was chosen to obtain those collection curves and net collection currents on the substrate electrode as shown in Figure 4. On the tip electrode, 0.4 mM DMA was electro-oxidized to form the DMA$^{\bullet+}$ by sweeping the tip potential, E_{tip}, from 0.6 to 1.3 V vs Ag QRE, while the substrate potential, E_{sub}, was held constant at 0.76 V vs Ag QRE to reduce DMA$^{\bullet+}$ back to DMA on the substrate UME. E_{sub} is a key parameter for the TG/SC mode of SECM. In this experiment, the DMA oxidation peak potential is around 0.92 V, and an almost constant oxidation background current is present when the potential is less than 0.78 V. At a more negative potential, the

Table 1. Boundary Conditions in the SECM Simulation[a]

no.	z coordinate	r coordinate	boundary conditions
1	10 μm + d	$0 \le r \le a$	$C_B = 0$; $D_B\frac{\partial C_B}{\partial z} = -D_A\frac{\partial C_A}{\partial z}$; $D_D\frac{\partial C_D}{\partial z} = -D_C\frac{\partial C_C}{\partial z} + D_E\frac{\partial C_E}{\partial z}$
2	10 μm + d	$a \le r \le r_{t1}$	$D_A\frac{\partial C_A}{\partial z} = D_B\frac{\partial C_B}{\partial z} = D_C\frac{\partial C_C}{\partial z} = D_D\frac{\partial C_D}{\partial z} = D_E\frac{\partial C_E}{\partial z} = 0$
3	$\frac{40 - d}{r_{t2} - r_{t1}}r + \frac{(10 + d)r_{t2} - 50r_{t1}}{r_{t2} - r_{t1}}$	$r_{t1} \le r \le r_{t2}$	$D_A\frac{\partial C_A}{\partial z} = D_B\frac{\partial C_B}{\partial z} = D_C\frac{\partial C_C}{\partial z} = D_D\frac{\partial C_D}{\partial z} = D_E\frac{\partial C_E}{\partial z} = 0$
4	50 μm	$r_{t2} \le r \le 50$ μm	$C_A = 0$; $C_B = C_B^*$; $C_{C-E} = 0$
5	10 μm	$0 \le r \le a'$	$C_A = 0$; $D_A\frac{\partial C_A}{\partial z} = -D_B\frac{\partial C_B}{\partial z}$; $D_D\frac{\partial C_D}{\partial z} = -D_C\frac{\partial C_C}{\partial z} + D_E\frac{\partial C_E}{\partial z}$
6	10 μm	$a' \le r \le r_{s1}$	$D_A\frac{C_A}{\partial z} = D_B\frac{\partial C_B}{\partial z} = D_C\frac{\partial C_C}{\partial z} = D_D\frac{\partial C_D}{\partial z} = D_E\frac{\partial C_E}{\partial z} = 0$
7	$\frac{-10}{r_{s2} - r_{s1}}r + \frac{10r_{s2}}{r_{s2} - r_{s1}}$	$r_{s1} \le r \le r_{s2}$	$D_A\frac{\partial C_A}{\partial z} = D_B\frac{\partial C_B}{\partial z} = D_C\frac{\partial C_C}{\partial z} = D_D\frac{\partial C_D}{\partial z} = D_E\frac{\partial C_E}{\partial z} = 0$
8	0 μm	$r_{s2} \le r \le 50$ μm	$C_A = 0$; $C_B = C_B^*$; $C_{C-E} = 0$
9	$0 \le z \le 50$ μm	$r = 50$ μm	$C_A = 0$; $C_B = C_B^*$; $C_{C-E} = 0$
10	10 μm $\le z \le$ 10 μm + d	$r = 0$	$D_A\frac{\partial C_A}{\partial r} = D_B\frac{\partial C_B}{\partial r} = D_C\frac{\partial C_C}{\partial r} = D_D\frac{\partial C_D}{\partial r} = D_E\frac{\partial C_E}{\partial r} = 0$

[a] r and z are the coordinates in the radial and normal directions to the electrode surface at its center, respectively. r_{t1}, r_{t2}, r_{s1}, and r_{s2} are characteristic parameters for the tip and the substrate as shown in Figure S6. D_i and C_i are the diffusion coefficients and concentrations of the two species, and t is time [i = A, B, C, D, and E; species i: (A) DMA$^{\bullet+}$, (B) DMA, (C) TMB, (D) TMB$^{\bullet+}$, (E) TMB^{2+}].

dimerization product of DMA$^{\bullet+}$ can be reduced, as shown in the CV curves in Figure 2a. Therefore, the substrate was held at 0.76 V. DMA$^{\bullet+}$ can be collected at the substrate electrode when d is sufficiently small.

To interpret the tip and substrate current curves at different d values, as shown in Figure 4b, it is necessary to account for the production of three oxidation products at the tip, DMA$^{\bullet+}$, TMB$^{\bullet+}$, and TMB^{2+}, and their reduction at the substrate as a function of d. This is accounted for in the simulations described below. However, the curves in Figure 4a yield direct evidence that DMA$^{\bullet+}$ is produced at steady state using the TG/SC mode of SECM.

The DMA oxidation currents on the tip and the corresponding collection currents on the substrate (baseline subtraction by linear fitting is shown in Figure 4a) with different gap distances d and the tip current at 1.3 V vs Ag QRE are shown in Figure 4b. The collection current of the DMA$^{\bullet+}$ on the substrate increases as d decreases from 1.4 to 0.2 μm, indicating that more and more DMA$^{\bullet+}$ is captured. The tip oxidation current is almost the same when the distance is high than 0.5 μm. With the distance decreasing to 0.2 μm, an obvious positive feedback effect can be found. The CE curve is shown in Figure 5. As d decreases from 1.4 to 0.2 μm, the CE increases from 0.17 to 0.90, indicating that almost all DMA$^{\bullet+}$ is captured at d = 0.2 μm at steady state.

DMA Oxidation Reaction Mechanism and Kinetic Parameters for the Irreversible Homogeneous Reaction. When d is large, the oxidation product of DMA predominantly forms TMB because of the high dimerization rate compared to the DMA$^{\bullet+}$ arrival at the substrate (routes 1 vs 2 in Figure 1). When d decreases to small enough values, more DMA$^{\bullet+}$ is detected on the substrate. Thus, collection efficiency depends not only on d, but also on k_c, as shown in Figure 5. Simulations were carried out with Multiphysics v4.2 software (COMSOL, Inc., Burlington, MA) as described in the Supporting Information. The simulation space was rendered in 2D axial symmetrical mode for a tip with a radius of 0.5 μm, RG = 2, and a substrate with a radius of 5 μm, RG = 3, vertically aligned in a cylinder with a radius of 50 μm and a height of 50 μm, as shown in Supporting Information, Figure S6. A depiction of the EC_2EE simulation model and corresponding boundary conditions in the TG/SC mode are shown in Table 1, and

Table 2. Reaction Mechanism and Corresponding Relevant Time-Dependent Diffusion Equation in Cylindrical Coordinates[a]

Reactions and Parameters	
$B - e^- \leftrightharpoons A$	$E^0 = 0.98$ V, $a = 0.5$, $k^0 = 1$ cm·s^{-1}
$2A \rightarrow C$	$k_c = 2.5 \times 10^8$ M^{-1}·s^{-1}
$C - e^- \leftrightharpoons D$	$E^0 = 0.59$ V, $a = 0.5$, $k^0 = 1$ cm·s^{-1}
$D - e^- \leftrightharpoons E$	$E^0 = 0.74$ V, $a = 0.5$, $k^0 = 1$ cm·s^{-1}

Relevant Time-Dependent Diffusion Equations

(1) $$\frac{\partial C_A}{\partial t} = D_A\left[\frac{\partial^2 C_A}{\partial r^2} + \frac{1}{r}\frac{\partial C_A}{\partial r} + \frac{\partial^2 C_A}{\partial z^2}\right] - k_c C_A{}^2$$

(2) $$\frac{\partial C_B}{\partial t} = D_A\left[\frac{\partial^2 C_B}{\partial r^2} + \frac{1}{r}\frac{\partial C_B}{\partial r} + \frac{\partial^2 C_B}{\partial z^2}\right]$$

(3) $$\frac{\partial C_C}{\partial t} = D_C\left[\frac{\partial^2 C_C}{\partial r^2} + \frac{1}{r}\frac{\partial C_C}{\partial r} + \frac{\partial^2 C_C}{\partial z^2}\right] + k_c C_A{}^2$$

(4) $$\frac{\partial C_D}{\partial t} = D_D\left[\frac{\partial^2 C_D}{\partial r^2} + \frac{1}{r}\frac{\partial C_D}{\partial r} + \frac{\partial^2 C_D}{\partial z^2}\right]$$

(5) $$\frac{\partial C_E}{\partial t} = D_E\left[\frac{\partial^2 C_E}{\partial r^2} + \frac{1}{r}\frac{\partial C_E}{\partial r} + \frac{\partial^2 C_E}{\partial z^2}\right]$$

Initial Condition, Completing the Definition of the Problem

$t = 0$, all r, z: $C_B = C_B{}^* = 0.4$ mM, $C_A = 0$, $C_{C-E} = 0$, $D_{A-E} = 2.4 \times 10^{-5}$ cm^2/s[b]
$E_{tip} = 1.3$ V, $E_{sub} = 0.76$ V

Current on the Tip (i_T) and Substrate (i_S)

$$i_T = 2\pi F D_B \int_0^a \left(\frac{\partial C_B}{\partial z}\right)_{z=0} r\,dr + 2\pi F D_C \int_0^a \left(\frac{\partial C_C}{\partial z}\right)_{z=0} r\,dr + 2\pi F D_D \int_0^a \left(\frac{\partial C_D}{\partial z}\right)_{z=0} r\,dr$$

$$i_S = 2\pi F D_A \int_0^{a'} \left(\frac{\partial C_A}{\partial z}\right)_{z=0} r\,dr - 2\pi F D_C \int_0^{a'} \left(\frac{\partial C_C}{\partial z}\right)_{z=0} r\,dr - 2\pi F D_D \int_0^{a'} \left(\frac{\partial C_D}{\partial z}\right)_{z=0} r + 2\pi F D_E \int_0^{a'} \left(\frac{\partial C_E}{\partial z}\right)_{z=0} r$$

[a] r and z are the coordinates in the radial and normal directions to the electrode surface at its center, respectively. D_i and C_i are the diffusion coefficients and concentrations of the species i, and t is time [i = A, B, C, D, and E; species i: (A) DMA$^{\bullet+}$, (B) DMA, (C) TMB, (D) TMB$^{\bullet+}$, (E) TMB^{2+}]. [b] DMA diffusion coefficient data from our previous work,[14] while other species' diffusion coefficients are assumed to be the same as that of DMA.

the reaction mechanism (a reversible electrochemical reaction followed by a second-order irreversible chemical reaction and a two-step electrochemical reaction, as shown in eqs 1−4). The corresponding relevant time-dependent diffusion equations in cylindrical coordinates are listed in Table 2. The COMSOL report is available in the Supporting Information.

The best fits of the CE curve as a function of d, with EC_2EE models for a given rate constant (k_c) for the dimerization reaction, are shown in Figure 5, along with the corresponding experimental CE curve. In the simulation the TMB oxidation reactions were assumed to be diffusion controlled with the standard potentials of 0.98, 0.59, and 0.74 V vs Ag QRE for DMA oxidation, TMB oxidation, and TMB$^{\bullet+}$ oxidation, respectively, based on the CV in Figure 2 and CV simulation by DigiElch,[18] since the DMA oxidation reaction is not a reversible reaction. Here, all electrochemical standard rate constants k^0 and transfer coefficients are assumed to be 1 cm·s^{-1} and 0.5, respectively, consistent with one-electron transfers for aromatic compounds in aprotic media.[35] Comparing the simulated and experimental data indicates that k_c is about 2.5×10^8 M^{-1}·s^{-1} based on the entire d region from 1.4 to 0.2 μm. The deviation between experimental data and simulation result is small, and almost all generated current on the tip can be collected on the substrate when d is 0.2 μm. For 0.4 mM DMA, this indicates a half-life of the radical cation of around 10 μs, which is too short to determine by FSCV.

For a second-order reaction, performing experiments at different reactant concentrationsare an effective way to obtain more information about the reaction mechanism. In the current study, we have tried to collect the DMA$^{\bullet+}$ with higher and lower concentrations of DMA than a single value, e.g., 1 mM and 0.1 mM. However, for concentrations >0.4 mM, the dimerization is too fast to obtain a good CE, even with a 200 nm gap. For lower concentrations, since the radius of tip is 0.5 μm, the corresponding tip and substrate collection currents are too small (a few tens of picoamperes) to obtain reliable measurements. We hope to achieve smaller gaps in the future, which will allow studies over a larger range of concentrations.

CONCLUSION

The TG/SC mode of SECM, with the tip and the substrate placed several hundred nanometers apart, was successfully applied to detect the short-lived intermediate radical cation DMA$^{\bullet+}$ in nonaqueous solution. This study represents the first direct detection of the DMA$^{\bullet+}$ and indicates that the electrochemical oxidation of DMA is followed by the dimerization of the radical cation. Since the SECM measurement can be conducted under steady state, but under a short time window, without the problem of capacitive charging, current that affect measurements like FSCV can be avoided. We find that, combined with simulations based on the proposed mechanism, the irreversible chemical reaction rate constant of DMA$^{\bullet+}$ dimerization is 3 orders of magnitude larger than the value estimated from FSCV.

ASSOCIATED CONTENT

Supporting Information

UME image and corresponding CV and approach curve, alignment of tip and substrate, the original collection curve, and COMSOL model report. This material is available free of charge via the Internet at http://pubs.acs.org.

AUTHOR INFORMATION

Corresponding Author

ajbard@mail.utexas.edu

Notes

The authors declare no competing financial interest.

ACKNOWLEDGMENTS

We acknowledge support of this research from the AFOSR MURI (FA9550-14-1-0003) and the Welch Foundation (F-0021). F.C. is especially grateful for the support of the China Scholarship Council, Zhejiang University New Star Project and National Natural Science Foundation of China (51171172). F.C. thanks Dr. Hong Zhao for discussion of the COMSOL simulation, Dr. Jinho Chang, Brent Bennett, Netzahualcóyotl Arroyo-Currás for help with the SECM experiment.

REFERENCES

(1) Yano, J. *J. Electrochem. Soc.* **1991**, *138*, 455.
(2) Weinberg, N. L.; Reddy, T. B. *J. Am. Chem. Soc.* **1968**, *90*, 91.
(3) Roy, P. R.; Saha, M. S.; Okajima, T.; Ohsaka, T. *Electrochim. Acta* **2006**, *51*, 4447.
(4) Roy, P. R.; Okajima, T.; Ohsaka, T. *J. Electroanal. Chem.* **2004**, *561*, 75.
(5) Parker, V. D.; Tilset, M. *J. Am. Chem. Soc.* **1991**, *113*, 8778.
(6) Park, S. G.; Trulove, P. C.; Carlin, R. T.; Osteryoung, R. A. *J. Am. Chem. Soc.* **1991**, *113*, 3334.
(7) Oyama, N.; Ohsaka, T.; Shimizu, T. *Anal. Chem.* **1985**, *57*, 1526.
(8) Oyama, M.; Higuchi, T. *J. Electrochem. Soc.* **2002**, *149*, E12.
(9) Ocon, P.; Herrasti, P. *J. Mater. Sci.* **1991**, *26*, 6487.
(10) Lapin, E.; Jureviciute, I.; Mazeikiene, R.; Niaura, G.; Malinauskas, A. *Synth. Met.* **2010**, *160*, 1843.
(11) Kirchgessner, M.; Sreenath, K.; Gopidas, K. R. *J. Org. Chem.* **2006**, *71*, 9849.
(12) Hand, R.; Nelson, R. F. *J. Electrochem. Soc.* **1970**, *117*, 1353.
(13) Mizoquchi, T.; Adams, R. N. *J. Am. Chem. Soc.* **1962**, *84*, 2058.
(14) Yang, H. J.; Wipf, D. O.; Bard, A. J. *J. Electroanal. Chem.* **1992**, *331*, 913.
(15) Seo, E. T.; Nelson, R. F.; Fritsch, J. M.; Marcoux, L. S.; Leedy, D. W.; Adams, R. N. *J. Am. Chem. Soc.* **1966**, *88*, 3498.
(16) Galus, Z.; Rowland, F. S.; White, R. M.; Adams, R. N. *J. Am. Chem. Soc.* **1962**, *84*, 2065.
(17) Galus, Z.; Adams, R. N. *J. Am. Chem. Soc.* **1962**, *84*, 2061.
(18) Chang, J. H.; Bard, A. J. *J. Am. Chem. Soc.* **2014**, *136*, 311.
(19) Bard, A. J.; Faulkner, L. R. *Electrochemical methods: fundamentals and applications*; John Wiley & Sons, Inc.: New York, 2001.
(20) Neubert, G.; Prater, K. B. *J. Electrochem. Soc.* **1974**, *121*, 745.
(21) Zhou, F. M.; Bard, A. J. *J. Am. Chem. Soc.* **1994**, *116*, 393.
(22) Bard, A. J.; Fan, F. R. F.; Kwak, J.; Lev, O. *Anal. Chem.* **1989**, *61*, 132.
(23) Bi, S. P.; Liu, B.; Fan, F. R. F.; Bard, A. J. *J. Am. Chem. Soc.* **2005**, *127*, 3690.
(24) Combellas, C.; Ghilane, J.; Kanoufi, F.; Mazouzi, D. *J. Phys. Chem. B* **2004**, *108*, 6391.
(25) Fan, F.-R. F.; Demaille, C. In *Scanning Electrochemical Microscopy*; Mirkin, M. V., Bard, A. J., Eds.; Marcel Dekker, Inc.: New York, 2001; p 75.
(26) Zhang, B.; Galusha, J.; Shiozawa, P. G.; Wang, G. L.; Bergren, A. J.; Jones, R. M.; White, R. J.; Ervin, E. N.; Cauley, C. C.; White, H. S. *Anal. Chem.* **2007**, *79*, 4778.
(27) Kim, J.; Kim, B. K.; Cho, S. K.; Bard, A. J. *J. Am. Chem. Soc.* **2014**, *136*, 8173.
(28) Katemann, B. B.; Schuhmann, T. *Electroanal* **2002**, *14*, 22.
(29) Kim, J.; Izadyar, A.; Nioradze, N.; Amemiya, S. *J. Am. Chem. Soc.* **2013**, *135*, 2321.
(30) Ishimatsu, R.; Kim, J.; Jing, P.; Striemer, C. C.; Fang, D. Z.; Fauchet, P. M.; McGrath, J. L.; Amemiya, S. *Anal. Chem.* **2010**, *82*, 7127.
(31) Bard, A. J.; Mirkin, M. V. *Scanning Electrochemical Microscopy*; Marcel Dekker: New York, 2001.
(32) Wain, A. J.; Pollard, A. J.; Richter, C. *Anal. Chem.* **2014**, *86*, 5143.
(33) Miao, W. J.; Ding, Z. F.; Bard, A. J. *J. Phys. Chem. B* **2002**, *106*, 1392.
(34) Shao, Y. H.; Mirkin, M. V. *J. Phys. Chem. B* **1998**, *102*, 9915.
(35) Kojima, H.; Bard, A. J. *J. Am. Chem. Soc.* **1975**, *97*, 6317.